Supporting Information: Magnetic Anisotropy of Individual Nanomagnets Embedded in Biological Systems Determined by Axi-Asymmetric X-Ray Transmission Microscopy

Lourdes Marcano*[1,2], Iñaki Orue[3], David Gandia[4], Lucía Gandarias[5], Markus Weigand[1], Radu Marius Abrudan[1], Ana García-Prieto[6], Alfredo García-Arribas[2,4], Alicia Muela[5], M. Luisa Fdez-Gubieda*[2,4], and Sergio Valencia*[1]

[1]Helmholtz-Zentrum Berlin für Materialien und Energie, Albert-Einstein-Str. 15, 12489 Berlin, Germany
[2]Dpto. Electricidad y Electrónica, Universidad del País Vasco - UPV/EHU, 48940 Leioa, Spain
[3]SGIker, Universidad del País Vasco - UPV/EHU, 48940 Leioa, Spain
[4]BCMaterials, Bld. Martina Casiano 3rd floor, 48940 Leioa, Spain
[5]Dpto. Inmunología, Microbiología y Parasitología, Universidad del País Vasco - UPV/EHU, 48940 Leioa, Spain
[6]Dpto. Física Aplicada, Universidad del País Vasco - UPV/EHU, 48013 Bilbao, Spain
*lourdes.marcano@ehu.eus; *malu.gubieda@ehu.eus; *sergio.valencia@helmholtz-berlin.de

April 19, 2022

S1 Macro- and Microscopic XAS and XMCD Spectroscopy Comparison

Figure S1 displays the comparison of the Fe L_3-edge XAS and XMCD spectra measured in transmission geometry on a macroscopic sample composed of a collection of randomly distributed cells with that obtained by STXM on a selected magnetosome chain. A movie showing the image sequence of the nonmagnetic x-ray absorption signal on the chain (XAS, computed as $(\sigma^+ + \sigma^-)$) recorded as a function of the photon energy, E, between 709 and 713 eV can be found in the Supporting Material. The maximum XMCD signal is obtained at 709.3 eV.

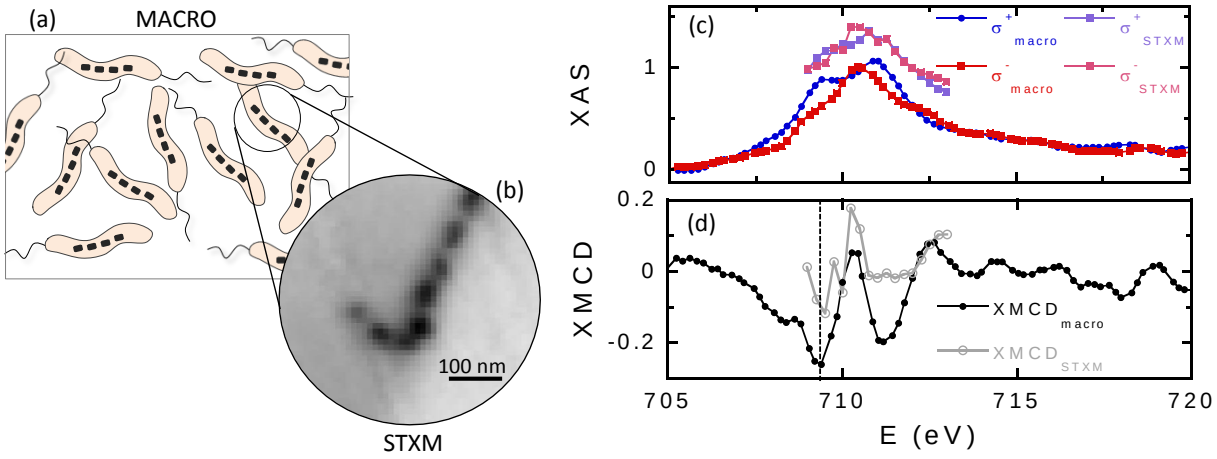

Figure S1: (a) Schematic representation of the collection of randomly distributed *M. blakemorei* cells ("macro") measured at ALICE station, beamline PM3 at HZB and (b) Space-resolved STXM-XAS image of an intracellular magnetosome chain collected at the Fe L_3-edge resonance energy (709.3 eV) acquired at MAXYMUS microscope, beamline UE46 at HZB. (c) Fe L_3-edge transmission x-ray absorption spectra macroscopically obtained ($\sigma^{\pm}_{\text{macro}}$) and on the selected intracellular magnetosome chain obtained by STXM-XMCD ($\sigma^{\pm}_{\text{STXM}}$). Spectra have been normalized by the maximum peak intensity at the L_3-edge of the nonmagnetic contribution of the x-ray absorption (XAS $= \sigma^+ + \sigma^-$). Computing $\sigma^- - \sigma^+$ gives the XMCD signal (d). The dotted line in (d) marks the energy at which the STXM images were recorded ($E = 709.3$ eV).

S2 Axi-Asymmetric Magnetic Field

Figure 2 within the main text displays the experimental magnetic field components, $\mu_0 H_y$ and $\mu_0 H_z$, and their dependence with the main component of the applied field, $\mu_0 H_x$. Experimental points have been fitted considering one or two ellipses, for $\mu_0 H_y$ and $\mu_0 H_z$, respectively. The analytical expresions of the fits are:

$$\mu_0 H_y = 2.5 - 13.679 \cdot \sqrt{1 - \left(\frac{\mu_0 H_x + 4.02}{261.58}\right)^2} \tag{1}$$

$$\mu_0 H_z = \left(-\frac{\mu_0 H_x - 40}{|\mu_0 H_x - 40|}\right) \cdot \left(14 \cdot \sqrt{\frac{1 - \left(\mu_0 H_x + \frac{\mu_0 H_x - 40}{|\mu_0 H_x - 40|} \cdot 40\right)^2}{300^2}} - 13.75\right) - 3.2 \tag{2}$$

where $\mu_0 H_{x,y,z}$ are in mT.

S3 Calculation of the Shape Magnetic Anisotropy Using Finite Elements Method

In order to accurately evaluate the observed magnetic behavior of magnetosomes in *Magnetovibrio blakemorei* MV-1 we have calculated the shape magnetic anisotropy associated to that morphology using Finite Elements Method (FEM).[5] A quantitative analysis of the magnetic shape anisotropy of an object involves the calculation of the magnetostatic energy density, E_{magn}, of the given shape:

$$E_{magn} = \oint -\frac{1}{2}\mu_0 \vec{H}_d \cdot \vec{M} dV \tag{3}$$

where $\vec{H}_d$ is the demagnetizing field, and $\vec{M}$ represents the magnetization vector. The integral extends to the whole volume of the object.

In single magnetic domain bodies, as in the case of magnetosomes, the magnetization $\vec{M}$ can be taken as uniform in the whole particle with the presence of free magnetic poles limited to its surface. Thus, within the particle, $\vec{M}$ can be kept constant along an arbitrary direction given by the unit vector $\hat{u}_m$,

$$\vec{M} = M \cdot \hat{u}_m \tag{4}$$

where M is set to the saturation magnetization of bulk magnetite (480 kA m^{-1}).

The magnetic poles distribution depends on the direction of the magnetization. The unit vector takes therefore the usual form in spherical coordinates.

$$\hat{u}_m = \sin\theta\cos\varphi\hat{i} + \sin\theta\sin\varphi\hat{j} + \cos\varphi\hat{k} \tag{5}$$

Thus, the magnetostatic energy density given by equation 3 is angle-dependent, enclosing the desired shape anisotropy.

The 3D-shape of the magnetosomes is modeled by considering a truncated hexa-octahedron extruded along the $[111]$ direction with an elongation degree (Width (W)/Length(L)) of approx-

imately 0.72 according to the bibliography[6] surrounded by air domain. To choose the desirable bounding conditions we imposed magnetic insulation at the ends of the air domain.[5]

On the other hand, the demagnetizing field $\vec{H}_d$ produced by the magnetization is calculated at all points inside the body using FEM. It is derived from the magnetostatic equations for a body with no currents:

$$\begin{aligned} \vec{B} &= \nabla \times \vec{A} \\ \nabla \times \vec{H} &= 0 \end{aligned} \tag{6}$$

being $\vec{A}$ the magnetic vector potential.

Together with the constitutive relationship:

$$\vec{B} = \mu_0(\vec{H} + \vec{M}) \tag{7}$$

we can calculate for our particular geometry both $\vec{B}$ and $\vec{H}$ fields for a single magnetization direction, evaluating the total magnetostatic energy density of the particle (equation 3).

This repetition is done in steps of 1°, from 0 to 180° for polar angle θ, and from 0 to 360° for azimuthal angle λ.[5]

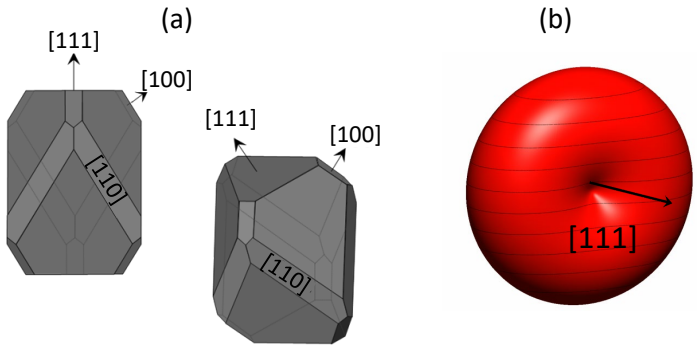

Figure S2: (a) Schematic representation of truncated hexa-octahedron, crystal habit of magnetosomes synthesized by *M. blakemorei*. (b) Shape anisotropy energy landscape of the truncated hexa-octahedral magnetosome system calculated by FEM method considering $W/L = 0.72$.

Following this procedure, we obtain the energy density landscape presented in Figure S2a. From the analysis of this landscape, we determine the easy axes, locating the energy minima,

and the anisotropy constants, from the energy barrier between the minima and maxima, and hence, the shape anisotropy of the magnetic nanoparticles. In the case of the truncated hexa-octahedron morphology there is only an absolute energy minimum located at the extruded $[111]$ direction (Figure S2a) with a calculated uniaxial anisotropy constant of $K_{\text{shape}} = 22$ kJ/m^3 for $W/L = 0.72$.

S4 Influence of the Cubic Magnetocrystalline Anisotropy of Magnetite in the Energy of the System

Figure S3 shows the zero-field anisotropy energy density landscapes considering two terms: the cubic magnetocrystalline anisotropy of magnetite with $K_{mc} = -11$ kJ/m^3 plus a uniaxial contribution along the long axis of the particle (a $\langle 111 \rangle$ crystallographic easy axis of magnetite) with an anisotropy constant K_u:

$$E_{anis}(\theta, \varphi) = E_{mc}(\theta, \varphi) + E_u(\theta, \varphi) = K_{mc}\left[\frac{\sin^4\theta \sin^2 2\varphi + \sin^2 2\theta}{4}\right] + K_u[1 - (\hat{u}_{111} \cdot \hat{u}_m)^2] \tag{8}$$

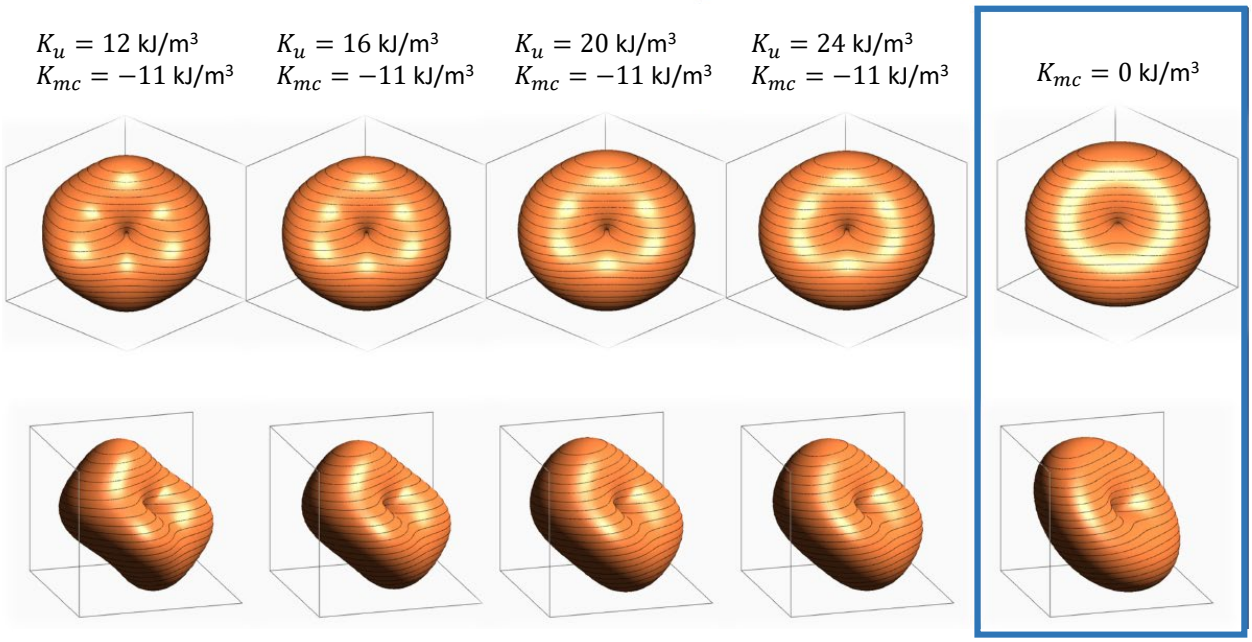

Figure S3: Zero-field energy landscapes of a truncated hexa-octahedral magnetosome as those of MV-1. The anisotropy energy comprises two terms: the cubic magnetocrystalline anisotropy of magnetite, with $K_{mc} = -11$ kJ/m^3 plus an effective uniaxial anisotropy term along the elongated crystallographic [111] axis that accounts for the shape anisotropy and dipolar interactions, characterized by an anisotropy constant K_u. The top and bottom rows are the same landscapes viewed from two different perspectives.

The uniaxial contribution accounts for the shape anisotropy and dipolar interactions be-

tween nearest neighbours. To highlight the effect of the cubic magnetocrystalline contribution on the total anisotropy energy, we have considered the range of values obtained from the simulations for the uniaxial effective anisotropy constant, from $K_u = 12$ kJ/m^3 to $K_u = 24$ kJ/m^3. Note that, according to the FEM simulations (see section S3), for an average truncated hexa-octahedral magnetosome with a width-to-length ratio $W/L = 0.72$, $K_{shape} = 22$ kJ/m^3, thus the shape anisotropy is the main contribution to the uniaxial term against the dipolar interactions, as expected. In Figure S3 we have also included for comparison the energy surface of a particle with a pure uniaxial anisotropy along the [111] axis with no cubic magnetocrystalline contribution ($K_{mc} = 0$), which yields a perfect toroid.

Figure S3 shows that even for the smallest value of $K_u = 12$ kJ/m^3, the energy surface has one single minimum, which means that the effective anisotropy is uniaxial regardless of the cubic magnetocrystalline anisotropy. Importantly, the position of this minimum, which defines the direction of the easy axis, is in all cases coincident with the elongated [111] direction. Thus, the cubic magnetocrystalline anisotropy deforms slightly the toroid along the other $\langle 111 \rangle$ directions, but it does not alter the uniaxial character of the anisotropy and neither tilts the easy axis, which remains along the elongated [111] direction. It does, however, add a small contribution to the effective uniaxial anisotropy constant of the system of the order of $K_{mc}/12 = 0.9$ kJ/m^3. As a result, in this system it is safe to evaluate the anisotropy energy density as an effective uniaxial anisotropy along the elongated [111] axis with an effective constant K which includes both the dominant shape anisotropy and dipolar interactions and the minor cubic magnetocrystalline contribution:

$$E_{anis}(\theta, \varphi) = K[1 - (\hat{u}_{111} \cdot \hat{u}_m)^2] \tag{9}$$

S5 Influence of the Axi-Asymmetric Magnetic Field and Geometry of the Experimental System on the Profile of the Hysteresis Loops

Firstly, aiming to understand the role of the axi-asymmetric magnetic field, Figure S4 depicts expected hysteresis loops based on the Stoner-Wohlfarth model depending on whether the magnetic field has only an x component (symmetric, $\mu_0 H_s$) or presents an axi-asymmetric component in y and z as described within the text ($\mu_0 H_a$). Note that, in our calculations, the applied magnetic field is entered as an input parameter in the simulations. The numerical simulations were carried out considering $\alpha = 90°$, an effective anisotropy constant $K = 20$ kJ/m^3 and different λ values.

Hysteresis loops corresponding to H_s are fully symmetric with respect to the axis. On the contrary the presence of an axi-asymmetric magnetic field leads to a shift of the loop along the field axis, which direction and strength depend on the sign and value of λ, respectively. That is, the axi-asymmetric field removes the degeneracy on the easy axis orientation ($\pm\lambda$) present with symmetric fields.

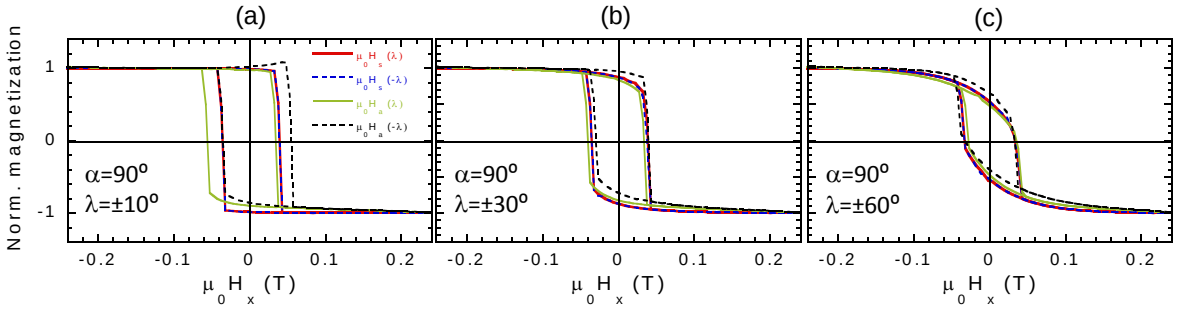

Figure S4: Simulated hysteresis loops calculated considering $\alpha = 90°$ and selected values of $\pm\lambda$ considering a symmetric applied field in the x direction ($\mu_0 H_s$) and the axi-asymmetric field used in the STXM measurements ($\mu_0 H_a$).

Secondly, to highlight the sensitivity of the local magnetic hysteresis to the magnetic easy

axis orientation we depict in Figure S5 magnetic hysteresis loops as function of polar (α) and azimuth (λ) angles of the magnetic easy axis considering an effective anisotropy constant of $K = 20$ kJ/m^3.

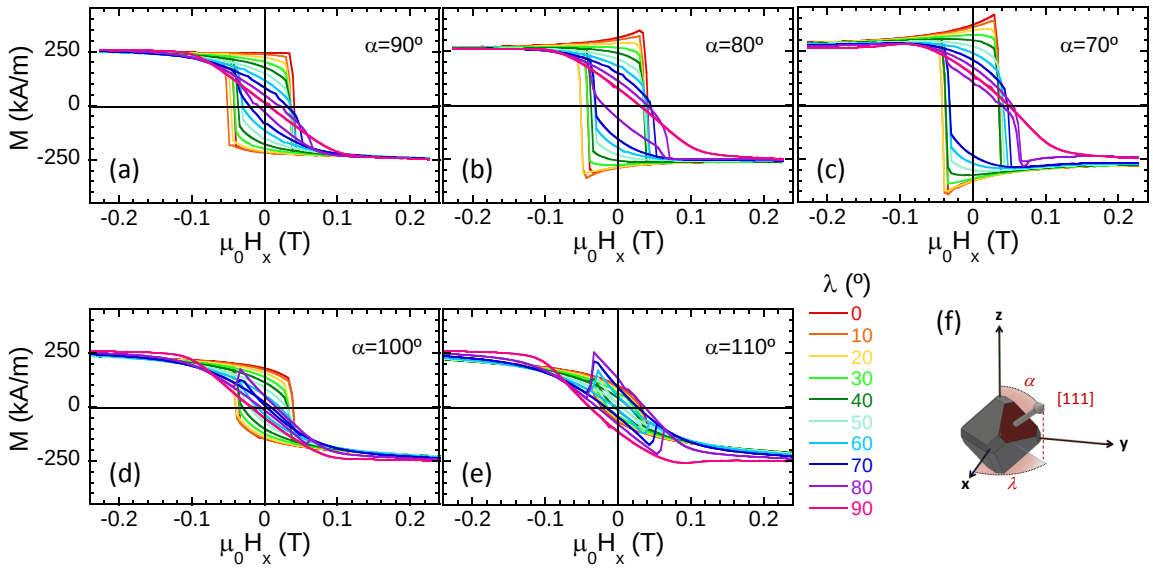

Figure S5: Simulated hysteresis loops calculated considering different values of λ and (a) $\alpha = 90°$, (b) 80°, (c) 70°, (d) 100° and (e) 110°. (f) Schematic representation of the geometry of the system, in which x,y and z denote the sample and magnetic field reference system and α and λ are the polar an azimuthal angles defining the orientation of the $[111]$ crystallographic direction of magnetite, coincident with the axis of elongation of the magnetosomes, with respect to the xyz reference system.

As shown in Figure S5, as α departs from 90°, the hysteresis loops start to distort. The high sensitivity of the hysteresis loops with α is due to the geometry of the experimental system itself, which is taken into account in the simulation. Indeed, the y axis of the hysteresis loop corresponds to the projection of the magnetization vector along the beam direction, that is, 120° off the xy sample plane (see Materials and Methods section). As the easy axis of the particle deviates from the xy-plane, the projection angle changes giving rise to the notable changes observed in Figure S5. Moreover, this experimental configuration also breaks down the otherwise existing symmetry of α with respect to the xy-plane (*i.e.* α=80° $\neq$ α=100°).

Note also that for λ=90° ($\mu_0 H_x$ field perpendicular to the magnetic easy axis) we observe that the shift of the hysteresis loops with respect to the field axis increases as α departs from the xy plane (α=90°), increasing the sensitivity of this parameter as well.

S6 Statistical Analysis of the RMSD Distribution

The probability distributions of K, α and λ for each particle have been calculated by following this protocol:

- The probability of a certain value of K is proportional to the number of simulations with that value of K whose RMSD lies below a certain confidence limit (in the text we have considered two confidence limits: 5% and 10% above RMSD_{min}).
- The probabilities of α and λ are calculated for a fixed value of K, the one corresponding to the best fit (RMSD_{min}). As in the previous case, the probability of a certain value of α (λ) is proportional to the number of simulations with that value of α (λ) whose RMSD lies below the confidence limit. For this, 2D matrices are analyzed, whose 3D representation for the case of particle 2 is presented in Figure 5d.

As an example, Figure S6 shows the probability distributions of K, α and λ for particle 2. These distributions give us a clear view of how reliable the determination of a given variable is. The average value of the distributions, represented as black squares (5%) and red spheres (10%) in Figures 5a,b,c of the main text, must be close enough to the value corresponding to the RMSD_{min} (asterisks). The standard deviation of the distribution can be taken as a measure of the uncertainty of a certain variable and is represented by black and red shadows in Figures 5a,b,c.

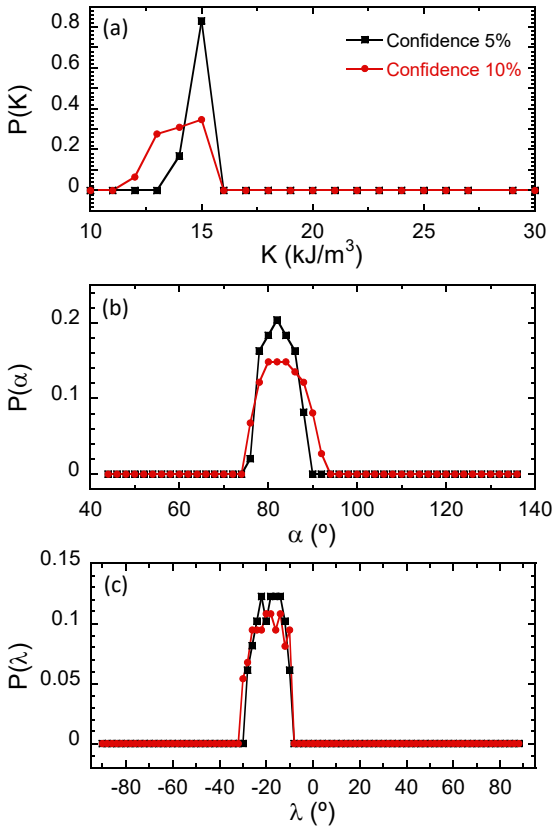

Figure S6: Probability distribution of K, α and λ which RMSD values are within RMSD_{min} and $\text{RMSD}_{\text{min}} + 5\%\text{RMSD}_{\text{min}}$ (black squares) and $\text{RMSD}_{\text{min}} + 10\%\text{RMSD}_{\text{min}}$ (red points) for magnetosome 2.

References

[1] R. Nakajima, J. Stöhr, Y. U. Idzerda, "Electron-Yield Saturation Effects in L-Edge X-Ray Magnetic Circular Dichroism Spectra of Fe, Co, and Ni," *Phys. Rev. B*, vol. 59, no. 9, pp. 6421–6429, 1999.

[2] S. Hanhan,A. M. Smith, M. Obst, A. P. Hitchcock, ´´Optimization of Analysis of Soft X-Ray Spectromicroscopy at the Ca 2p Edge," *J. Electron. Spectrosc. Relat. Phenom.*, vol. 173, no. 1, pp. 44–49, 2009.

[3] V. S. Coker, C. I. Pearce, C. Lang, G. Van Der Laan, Gerrit R. A. D. Pattrick, N. D. Telling, D. Schüler, E. Arenholz, J. R. Lloyd, "Cation Site Occupancy of Biogenic Magnetite Compared to Polygenic Ferrite Spinels Determined by X-Ray Magnetic Circular Dichroism," *Eur. J. Mineral.*, vol. 19, no. 5, pp. 707–716, 2007.

[4] F. Jiménez-Villacorta, C. Prieto,Y. Huttel,N. D. Telling, G. Van Der Laan, "X-Ray Magnetic Circular Dichroism Study of the Blocking Process in Nanostructured Iron-Iron Oxide Core-Shell Systems," *Phys. Rev. B*, vol. 84, no. 17, p. 172404, 2011.

[5] D. Gandia, L. Gandarias, L. Marcano, I. Orue, D. Gil-Cartón, J. Alonso, A. García-Arribas, A. Muela, and M. L. Fdez-Gubieda, "Elucidating the Role of Shape Anisotropy in Faceted Magnetic Nanoparticles Using Biogenic Magnetosomes as a Model," *Nanoscale*, vol. 12, no. 30, pp. 16081–16090, 2020.

[6] K. L. Thomas-Keprta, D. A. Bazylinski, J. L. Kirschvink, S. J. Clemett, D. S. Mckay, S. J. Wentworth, H. Vali, E. K. G. Jr, and C. S. Romanek, "Elongated Prismatic Magnetite Crystals in ALH84001 Carbonate Globules: Potential Martian Magnetofossils," *Geochim. Cosmochim. Acta*, vol. 64, no. 23, pp. 4049–4081, 2000.